Finite Element Models applied in Active Structural Acoustic Control

Marco H.H. Oude Nijhuis[a] and André de Boer[a]

[a]University of Twente, Department of Mechanical Engineering,
P.O. Box 217, 7500 AE Enschede, The Netherlands

ABSTRACT

This paper discusses the modelling of systems for active structural acoustic control. The finite element method is applied to model structures including the dynamics of piezoelectric sensors and actuators. A model reduction technique is presented to make the finite element model suitable for controller design. The reduced structural model is combined with an acoustic model which uses the radiation mode concept. For a test case consisting of a rectangular plate with one piezo patch the model reduction technique is validated. The results show that the an accurate prediction of both the structural and acoustic response is predicted by the reduced model. The model is compact requiring small simulation times, which makes it attractive for control system design. Finally the control performances for both structural and acoustic error criteria are presented.

Keywords: Active Structural Acoustic Control, piezoelectric materials, Finite Element Method, model reduction.

1. INTRODUCTION

Over the past decades, active control methods have become valuable tools besides passive methods for attenuation of structure borne sound. In active noise control the sound field introduced by a vibrating structure is cancelled using a control system with one or several speakers and error microphones. There are a number examples where this method is successfully applied, but noise reduction in a large spatial domain, here referred to as global control, is hard to achieve. In other words, it is only possible to create a small "quiet zone". A more promising method for global control which was first introduced by Fuller[1] is active structural acoustic control (Asac). In this method the actuators are directly attached to the structure, and a reduction of the radiated sound is achieved by changing the vibrational behaviour of the structure. Furthermore, often a control system is used with sensors which measure vibrations rather than acoustic pressure. Piezoelectric materials are often used in Asac as actuators and sensor, mainly because they can be bonded directly on the structure, and do not need a back support. Part of the research carried out worldwide focuses on modelling of Asac systems. With such a model the performance of a control algorithm can be determined a priori, or, it can be used to determine optimal sensor and actuator locations. For a small number of structures, such as rectangular plates, the dynamical behaviour can be described with analytical models (e.g. in Dimitriadis[2]). Unfortunately, this is not the case for many practical problems. Since active control is more valuable in the low frequency region, the Finite Element Method (Fem) can be applied for such problems. Furthermore, it is then possible to create models which include the actuator and sensor dynamics. This is in contrast to most analytical models.

This paper presents a method for developing models which describe the dynamical behaviour of structures with piezoelectric actuators and sensors. Fem models inherently have many degrees of freedom, and require therefore large simulation times. This is very impractical for control system design. A model reduction technique based on modal superposition is presented with special emphasis on the choice of the reduced base. The reduction technique is validated for a test case consisting of a rectangular plate with one piezoelectric actuator. A model to predict the sound radiation of the structure is added to the structural model. This work considers flat structures,

Further author information: (Send correspondence to M.H.H. Oude Nijhuis)
M.H.H. Oude Nijhuis: E-mail: m.h.h.oudenijhuis@wb.utwente.nl, Telephone: +31 53 489 5618
A. de Boer: E-mail: a.deboer@wb.utwente.nl

and therefore the Rayleigh integral is used for evaluation of the acoustic field. The concept of radiation modes is applied for an efficient evaluation of the radiated sound power. For the test case optimal control performances are presented for both structural and acoustic error criteria.

2. MODELLING OF ASAC SYSTEMS

In this section the FEM modelling approach of an arbitrary structure with piezoelectric sensors and actuators is presented. A model that describes the sound radiation of the structure will be introduced in Sect. 3. The linear FEM equations of motion for a coupled structural-piezoelectric system are given by

$$\begin{bmatrix} \mathbf{M}_{uu} & \mathbf{0} \\ \mathbf{0} & \mathbf{0} \end{bmatrix} \begin{Bmatrix} \ddot{\mathbf{u}} \\ \ddot{\boldsymbol{\phi}} \end{Bmatrix} + \begin{bmatrix} \mathbf{C}_{uu} & \mathbf{0} \\ \mathbf{0} & \mathbf{0} \end{bmatrix} \begin{Bmatrix} \dot{\mathbf{u}} \\ \dot{\boldsymbol{\phi}} \end{Bmatrix} + \begin{bmatrix} \mathbf{K}_{uu} & \mathbf{K}_{u\phi} \\ \mathbf{K}_{\phi u} & \mathbf{K}_{\phi\phi} \end{bmatrix} \begin{Bmatrix} \mathbf{u} \\ \boldsymbol{\phi} \end{Bmatrix} = \begin{Bmatrix} \mathbf{f} \\ \mathbf{g} \end{Bmatrix}, \tag{1}$$

where $\mathbf{u}$ is the vector with the nodal structural displacements and rotations, and $\boldsymbol{\phi}$ is the vector with nodal voltages. Matrices $\mathbf{M}_{uu}$, $\mathbf{C}_{uu}$, and $\mathbf{K}_{uu}$ are respectively the structural mass, damping and stiffness matrix. The piezoelectric coupling arises in the piezoelectric stiffness matrices $\mathbf{K}_{u\phi}$ and $\mathbf{K}_{\phi u} = \mathbf{K}_{u\phi}^{\mathrm{T}}$ and the dielectric stiffness matrix $\mathbf{K}_{\phi\phi}$. The external loads are stored in $\mathbf{f}$, i.e. the vector with nodal structural forces, and $\mathbf{g}$, which is the vector with nodal electrical charges. The symbols $\dot{}$ and $\ddot{}$ denote the first and second time derivatives. The main assumption made in the derivation of Eqs. (1) is that the electrical field behaves quasi-statically. This explains why the mass and damping matrix only contain structural contributions. Note that $\mathbf{u}$ contains the nodal displacements of the structure as well as the nodal displacements of the piezoelectric material. There exists various formulations for beam, plate and solid piezoelectric finite elements, of which an overview can be found in Benjeddou.[3]

2.1. Model Reduction

In general FEM models contain a large number of degrees of freedom (DOF). This feature makes such models not suitable for the design of a controller, since control system design is often an iterative procedure which requires many simulations. In this section a model reduction technique is presented for a dynamical system described by Eqs. (1). In a control setup piezoelectric materials can be used either as actuator or sensor. In case the patch is used as actuator the electrode potential is prescribed, whereas for a sensor the potential is free.* It is convenient to divide the vector with the nodal voltages into two parts: $\boldsymbol{\phi} = \{\boldsymbol{\phi}^p \ \boldsymbol{\phi}^f\}^{\mathrm{T}}$, where $\boldsymbol{\phi}^p$ is the vector with *prescribed* nodal voltages, and $\boldsymbol{\phi}^f$ contains the *free* nodal voltages. Substitution of this vector into Eqs. (1) gives

$$\begin{bmatrix} \mathbf{M}_{uu} & \mathbf{0} & \mathbf{0} \\ \mathbf{0} & \mathbf{0} & \mathbf{0} \\ \mathbf{0} & \mathbf{0} & \mathbf{0} \end{bmatrix} \begin{Bmatrix} \ddot{\mathbf{u}} \\ \ddot{\boldsymbol{\phi}}^p \\ \ddot{\boldsymbol{\phi}}^f \end{Bmatrix} + \ldots + \begin{bmatrix} \mathbf{K}_{uu} & \mathbf{K}_{u\phi}^p & \mathbf{K}_{u\phi}^f \\ \mathbf{K}_{\phi u}^p & \mathbf{K}_{\phi\phi}^{pp} & \mathbf{K}_{\phi\phi}^{pf} \\ \mathbf{K}_{\phi u}^f & \mathbf{K}_{\phi\phi}^{fp} & \mathbf{K}_{\phi\phi}^{ff} \end{bmatrix} \begin{Bmatrix} \mathbf{u} \\ \boldsymbol{\phi}^p \\ \boldsymbol{\phi}^f \end{Bmatrix} = \begin{Bmatrix} \mathbf{f} \\ \mathbf{g}^p \\ \mathbf{g}^f \end{Bmatrix}. \tag{2}$$

For ease of writing the damping forces are omitted in this equation. The reduction method discussed here is a *mode superposition method*. To perform a modal analysis the electrical DOF are eliminated from the system. With the third row in Eqs. (2) the free voltages can be written in terms of the displacements, the free charges, and prescribed voltages:

$$\boldsymbol{\phi}^f = \left(\mathbf{K}_{\phi\phi}^{ff}\right)^{-1} \left[\mathbf{g}^f - \mathbf{K}_{\phi u}^f \, \mathbf{u} - \mathbf{K}_{\phi\phi}^{fp} \, \boldsymbol{\phi}^p\right]. \tag{3}$$

Substitution of this equation into the first row in Eqs. (2) results to an equation of motion in terms of the structural displacements, i.e.

$$\mathbf{M}_{uu} \, \ddot{\mathbf{u}} + \mathbf{C}_{uu} \, \dot{\mathbf{u}} + \mathbf{K}_{uu}^{\star} \, \mathbf{u} = \mathbf{f}^{\star}, \tag{4}$$

where the effective stiffness matrix $\mathbf{K}_{uu}^{\star}$ is defined as,

$$\mathbf{K}_{uu}^{\star} = \mathbf{K}_{uu} - \mathbf{K}_{u\phi}^f \left(\mathbf{K}_{\phi\phi}^{ff}\right)^{-1} \mathbf{K}_{\phi u}^f. \tag{5}$$

*The charge can also be used as sensor signal, but this will not be discussed in this work.

The effective force vector $\mathbf{f}^\star$ is defined as

$$\mathbf{f}^\star = \mathbf{f} - \mathbf{K}^f_{u\phi}\big(\mathbf{K}^{ff}_{\phi\phi}\big)^{-1}\,\mathbf{g}^f - \mathbf{K}^{p\star}_{u\phi}\,\boldsymbol{\phi}^p\,, \tag{6}$$

where $\mathbf{K}^{p\star}_{u\phi} = \mathbf{K}^p_{u\phi} - \mathbf{K}^f_{u\phi}\big(\mathbf{K}^{ff}_{\phi\phi}\big)^{-1}\mathbf{K}^{fp}_{\phi\phi}$. This equation shows that all applied electrical loads, i.e. nodal charges and prescribed nodal voltages, are transformed to structural loads. It will be clear that once the structural response is determined, the free voltages can be calculated with Eq. (3). If necessary, the nodal charges corresponding with the prescribed voltages can be calculated with the second row in Eqs. (2).

In the mode superposition method, the response is expanded in terms of the undamped eigenvectors or mode shapes (modes) of the problem. In case the undamped free vibration is considered ($\mathbf{f}^\star = \mathbf{0}$), and harmonic time dependency is assumed ($\mathbf{u} = \hat{\mathbf{u}}\,\mathrm{e}^{\mathrm{j}\omega t}$)[†], Eq. (4) reduces to the generalized eigenvalue problem:

$$\omega^2\mathbf{M}_{uu}\,\hat{\mathbf{u}} = \mathbf{K}^\star_{uu}\,\hat{\mathbf{u}}\,, \tag{7}$$

where ω is the angular frequency of vibration. The solution of this eigenvalue problem comprises n angular eigenfrequencies ω_i and corresponding eigenvectors $\hat{\mathbf{u}}_i$ ($i = 1\ldots n$), where n is the total number structural DOF in the model. The matrix with natural eigenfrequencies and the modal matrix with structural responses are defined as

$$\boldsymbol{\Omega} = \begin{bmatrix} \omega_1 & 0 & \cdots & 0 \\ 0 & \omega_2 & \cdots & 0 \\ \vdots & \vdots & \ddots & \vdots \\ 0 & 0 & \cdots & \omega_n \end{bmatrix}, \qquad \boldsymbol{\Psi}_u = \begin{bmatrix} \hat{\mathbf{u}}_1 & \hat{\mathbf{u}}_2 & \cdots & \hat{\mathbf{u}}_n \end{bmatrix}. \tag{8}$$

The mode shapes are normalized with respect to the mass matrix, thus satisfying

$$\boldsymbol{\Psi}_u^{\mathrm{T}}\mathbf{M}_{uu}\,\boldsymbol{\Psi}_u = \mathbf{I}\,, \tag{9}$$

$$\boldsymbol{\Psi}_u^{\mathrm{T}}\mathbf{K}^\star_{uu}\,\boldsymbol{\Psi}_u = \boldsymbol{\Omega}^2\,, \tag{10}$$

where $\mathbf{I}$ is the identity matrix. The modal responses of the free voltages follow from Eq. (3) for the unforced case, i.e. $\mathbf{g}^f = \boldsymbol{\phi}^p = \mathbf{0}$. The modal matrix with electrical responses is thus defined as

$$\boldsymbol{\Psi}_f = -\big(\mathbf{K}^{ff}_{\phi\phi}\big)^{-1}\mathbf{K}^f_{\phi u}\,\boldsymbol{\Psi}_u\,. \tag{11}$$

Following the method of modal superposition, the solution of Eq. (4) is written as

$$\mathbf{u} = \sum_{i=1}^{n}\hat{\mathbf{u}}_i q_i = \boldsymbol{\Psi}_u\,\mathbf{q}\,, \tag{12}$$

where $\mathbf{q}$ is the column vector with modal participation factors or generalized co-ordinates. Substitution of this solution into Eq. (4) and multiplying through by $\boldsymbol{\Psi}_u^{\mathrm{T}}$ leads to the generalized equation of motion:

$$\mathbf{I}\,\ddot{\mathbf{q}} + 2\,\boldsymbol{\Xi}\,\boldsymbol{\Omega}\,\dot{\mathbf{q}} + \boldsymbol{\Omega}^2\,\mathbf{q} = \boldsymbol{\Psi}_u^{\mathrm{T}}\,\mathbf{f}^\star\,, \qquad \text{or,} \tag{13}$$

$$\ddot{q}_i + 2\xi_i\omega_i\,\dot{q}_i + \omega_i^2\,q_i = \hat{\mathbf{u}}_i^{\mathrm{T}}\mathbf{f}^\star\,, \qquad i = 1\ldots n\,. \tag{14}$$

It is here assumed that the damping is *classical*, which implies that the modal damping matrix $\boldsymbol{\Xi}$ is diagonal, i.e. $\boldsymbol{\Xi} = \mathrm{diag}(\xi_i)$ with ξ_i the modal damping ratio for mode i. The notation in Eqs. (13) and (14) is not valid if the damping is not classical, although a transformation to generalized co-ordinates is still possible. Often it is the goal to determine the response in a limited frequency band $\omega \in [0, \omega_b]$. Conveniently, it is not necessary to take into account all modes of the system for modal superposition. A good estimate of the response in the frequency range of interest is obtained when only a small number of mode shapes is taken into account. When m eigenfrequencies and eigenvectors are included with $m \ll n$, the structural response in the frequency domain is approximated by

$$\hat{\mathbf{u}} \approx \sum_{i=1}^{m}\frac{\hat{\mathbf{u}}_i\,\hat{\mathbf{u}}_i^{\mathrm{T}}\mathbf{f}^\star}{-\omega^2 + 2\mathrm{j}\xi_i\omega_i\,\omega + \omega_i^2}\,. \tag{15}$$

[†] $\mathrm{j} = \sqrt{-1}$ is the imaginary unit.

2.2. Residual Flexibility

A consequence of truncating the modal expansion is that it can lead to errors in prediction the response near the anti-resonance frequencies, or in control theory referred to as *zeros*.[4] This is because the mode shapes with eigenfrequencies outside the frequency range of interest also contribute to the frequency response in the range $[0, \omega_b]$. This contribution is especially significant in the off-resonance regions. The concept of *residual flexibility* improves the accuracy of the truncated expansion. It is most easily explained when considering the frequency domain response. The exact solution of Eq. (4) when all variables show harmonic time dependency can be written as

$$\hat{\mathbf{u}} = \sum_{i=1}^{m} \hat{\mathbf{u}}_i \hat{q}_i + \sum_{i=m+1}^{n} \hat{\mathbf{u}}_i \hat{q}_i \,, \qquad \text{where} \qquad \hat{q}_i = \frac{\hat{\mathbf{u}}_i^{\mathrm{T}} \mathbf{f}^\star}{-\omega^2 + 2\mathrm{j}\xi_i \omega_i \, \omega + \omega_i^2} \,. \tag{16}$$

In the case of standard modal reduction, the second right-hand-side term is neglected (see Eq. (15)). Since the maximum frequency in the range of interest $[0, \omega_b]$ is much smaller than the natural eigenfrequencies for modes satisfying $i > m$, the system response is well approximated by

$$\hat{\mathbf{u}} \approx \sum_{i=1}^{m} \frac{\hat{\mathbf{u}}_i \hat{\mathbf{u}}_i^{\mathrm{T}} \mathbf{f}^\star}{-\omega^2 + 2\mathrm{j}\xi_i \omega_i \, \omega + \omega_i^2} + \sum_{i=m+1}^{n} \frac{\hat{\mathbf{u}}_i \hat{\mathbf{u}}_i^{\mathrm{T}} \mathbf{f}^\star}{\omega_i^2} \,. \tag{17}$$

In this approximation the high frequency modes ($i > m$) contribute statically to the system response, whereas the low frequency modes ($i \leq m$) respond dynamically. The second right-hand-side term is called the residual flexibility. In general only the eigenfrequencies and corresponding mode shapes for $i = 1 \ldots m$ are calculated when a modal analysis is performed with a FEM package. The residual flexibility can be expressed in terms of the static response and low frequency mode contributions. The modal expansion of the static response simply follows after inserting $\omega = 0$ into Eq. (16). Now the approximate solution becomes

$$\hat{\mathbf{u}} \approx \sum_{i=1}^{m} \frac{\hat{\mathbf{u}}_i \hat{\mathbf{u}}_i^{\mathrm{T}} \mathbf{f}^\star}{-\omega^2 + 2\mathrm{j}\xi_i \omega_i \, \omega + \omega_i^2} + \mathbf{u}_0 - \sum_{i=1}^{m} \frac{\hat{\mathbf{u}}_i \hat{\mathbf{u}}_i^{\mathrm{T}} \mathbf{f}^\star}{\omega_i^2} \,. \tag{18}$$

Solution $\hat{\mathbf{u}}$ is now written in terms of modes $i = 1 \ldots m$ and the static response $\mathbf{u}_0$. So the cost for a more accurate approximation is that a static response analysis has to be performed. The approach was here explained for a structure which has no rigid body modes. For a discussion on systems with rigid body modes, the reader is referred to Preumont.[4] In matrix-vector notation, Eq. (18) reads

$$\mathbf{u} \approx \tilde{\boldsymbol{\Psi}}_u \, \tilde{\mathbf{q}} + \mathbf{u}_0 - \tilde{\boldsymbol{\Psi}}_u \, \tilde{\boldsymbol{\Omega}}^{-2} \, \tilde{\boldsymbol{\Psi}}_u^{\mathrm{T}} \, \mathbf{f}^\star \,, \tag{19}$$

where $\tilde{\boldsymbol{\Omega}}^{-2} = \mathrm{diag}(\omega_i^{-2})$. In this equation the $\tilde{}$ symbol indicates that only modes $1 \ldots m$ are included. If this equation is inserted into Eq. (3) and some terms are rearranged, the following expression for the response of the free voltages is found:

$$\boldsymbol{\phi}^f \approx \tilde{\boldsymbol{\Psi}}_f \tilde{\mathbf{q}} + \boldsymbol{\phi}_0^f - \tilde{\boldsymbol{\Psi}}_f \, \tilde{\boldsymbol{\Omega}}^{-2} \, \tilde{\boldsymbol{\Psi}}_u^{\mathrm{T}} \, \mathbf{f}^\star \,, \tag{20}$$

where $\boldsymbol{\phi}_0^f$ is the vector with the static response of the free voltages.

2.3. State Space Representation

The foregoing model is rewritten in state space form since this form is more convenient for control system design. The general state space representation of any linear dynamical system is given by

$$\dot{\mathbf{x}} = \mathbf{A}\,\mathbf{x} + \mathbf{B}\,\mathbf{v} \,, \tag{21}$$

$$\mathbf{y} = \mathbf{C}\,\mathbf{x} + \mathbf{D}\,\mathbf{v} \,. \tag{22}$$

The modal participation factors are used to define state vector; i.e. $\mathbf{x} = \{\tilde{\mathbf{q}} \;\; \dot{\tilde{\mathbf{q}}}\}^{\mathrm{T}}$. The input vector containing all external inputs acting on the system, i.e. forces, charges and prescribed voltages is defined as $\mathbf{v} = \{\mathbf{f} \;\; \mathbf{g}^f \;\; \boldsymbol{\phi}^p\}^{\mathrm{T}}$. The system matrix and input matrix are defined as

$$\mathbf{A} = \begin{bmatrix} \mathbf{0} & \mathbf{I} \\ -\tilde{\boldsymbol{\Omega}}^2 & -2\,\tilde{\boldsymbol{\Xi}}\,\tilde{\boldsymbol{\Omega}} \end{bmatrix}, \qquad \mathbf{B} = \begin{bmatrix} \mathbf{0} & \mathbf{0} & \mathbf{0} \\ \tilde{\boldsymbol{\Psi}}_u^{\mathrm{T}} & \tilde{\boldsymbol{\Psi}}_f^{\mathrm{T}} & -\tilde{\boldsymbol{\Psi}}_u^{\mathrm{T}}\,\mathbf{K}_{u\phi}^{p\star} \end{bmatrix}. \tag{23}$$

Here the output vector is defined as $\mathbf{y} = \{\mathbf{u} \;\; \boldsymbol{\phi}^f\}^{\mathrm{T}}$. The nodal displacement vector is here an output, but the velocity or acceleration can also be used. The corresponding output and feedthrough matrix are given by

$$\mathbf{C} = \begin{bmatrix} \bar{\boldsymbol{\Psi}}_u & \mathbf{0} \\ \bar{\boldsymbol{\Psi}}_f & \mathbf{0} \end{bmatrix}, \qquad \mathbf{D} = \begin{bmatrix} \mathbf{U}_0 \\ \boldsymbol{\Phi}_0 \end{bmatrix} - \begin{bmatrix} \bar{\boldsymbol{\Psi}}_u \\ \bar{\boldsymbol{\Psi}}_f \end{bmatrix} \bar{\boldsymbol{\Omega}}^{-2} \begin{bmatrix} \bar{\boldsymbol{\Psi}}_u^{\mathrm{T}} & \bar{\boldsymbol{\Psi}}_f^{\mathrm{T}} & -\bar{\boldsymbol{\Psi}}_u^{\mathrm{T}}\,\mathbf{K}_{u\phi}^{p\star} \end{bmatrix}, \tag{24}$$

The residual flexibility is accounted for in the feedthrough matrix. In matrices $\mathbf{U}_0$ and $\boldsymbol{\Phi}_0$ every column i represents the static response when input i is equal to one whereas all other inputs are zero. In general, the number of inputs and outputs are much smaller than the number of DOF in the model. In the foregoing this aspect was not accounted for, i.e. the modal matrices contain the response of all DOF. The state space model can be written more compact when only those parts of the modal matrices are included which correspond with input or output DOF. The results presented in the next section were determined with a state space model implemented in such a way.

2.4. Test Case Results

The model reduction method is validated for a test case consisting of a clamped rectangular plate with one surface bonded piezoelectric patch actuator, see Fig. 1. The plate dimensions are $490 \times 245 \times 1.2$ mm^3 and the piezo is of size $50 \times 30 \times 1.0$ mm^3. Other test case properties are listed in App. A. Harmonic analysis results of the reduced models with and without residual flexibility are compared to results obtained with the full FEM model, i.e. directly solving Eq. (1). The model was constructed in the commercial finite element package ANSYS.

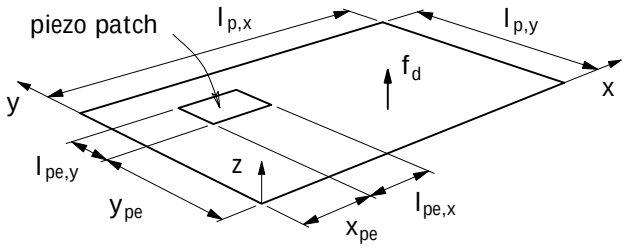

Figure 1: Clamped rectangular plate with one piezoelectric patch.

The plate is modelled with linear quadrilateral shell elements (SHELL63). In ANSYS no shell type elements with piezoelectric coupling are available, and therefore the piezo patches are modelled with linear cubic solid elements (SOLID5). In order to couple the solid and shell elements coupling conditions are introduced equivalent with perfect bonding between the plate and the piezo patch. The state space formulation of the reduced model has been implemented in MATLAB/SIMULINK. Besides the eigenfrequencies and modeshapes also piezoelectric stiffness matrices are required to define the reduced model. A number of routines to import the ANSYS model data and results were implemented in MATLAB.

The frequency response functions (FRF) for two load cases are considered. In the first case the plate is excited with a point force acting in the z-direction, whereas the piezo patch is short circuited. The force is applied at co-ordinates $(x, y) = (75, 158)$ mm. In the second case the plate is excited by a prescribed voltage applied to the top electrode of the piezo patch, whereas the bottom electrode is grounded. It is noted that the point force location and the piezo patch location were chosen such that all mode shapes in the frequency range

up to 500 Hz are excited. A total of 12 eigenfrequencies and mode shapes were included in the reduced model. The results for the first load case are shown in Fig. 2. Figure 2(a) shows the transfer between the point force and the transverse displacement at the location where this force is applied. It can be observed that for both reduced models the transfer function near the resonance frequencies is accurately described. Near the anti-resonance frequencies, i.e. the zeros, the reduced model including residual flexibility shows a better correspondence. One should be aware of the fact that the number of zeros and the corresponding frequencies are unique for every response point. Because in Fig. 2(a) the response point is equal to the excitation point, between every pair of resonances an anti-resonance frequency is present.

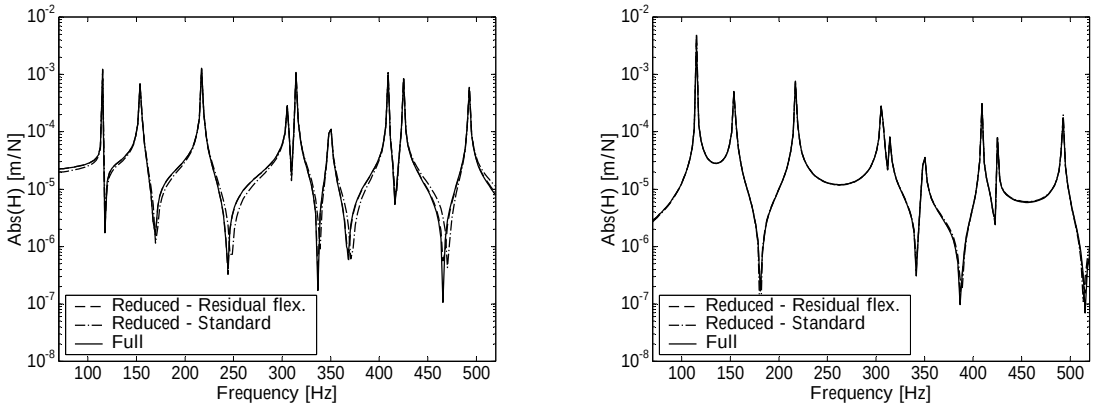

(a) Point force location

(b) Center of piezo patch

Figure 2: Transfer functions between point force and plate response.

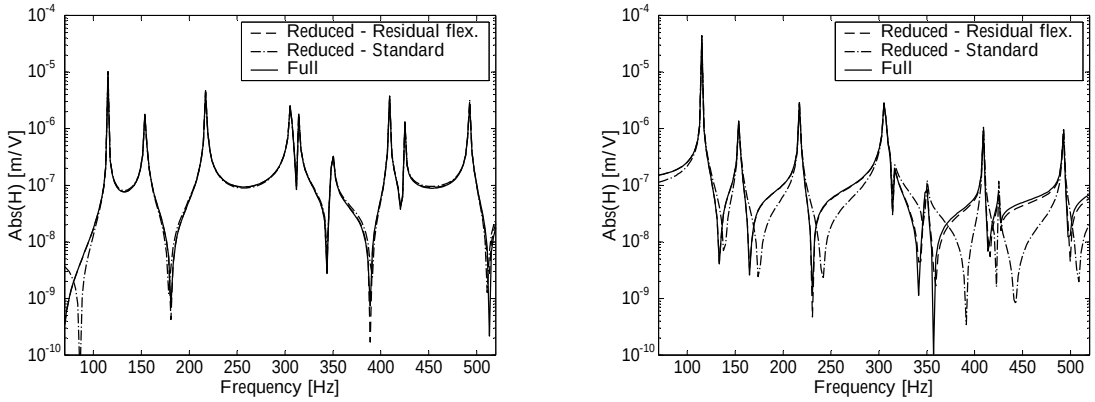

(a) Point force location

(b) Center of piezo patch

Figure 3: Transfer functions between piezo voltage and plate response.

Figure 2(b) shows the transfer between the point force and the transverse displacement at the center of the piezo patch. The effect of residual flexibility is negligible in this case as the three lines are nearly identical. The difference introduced by the residual flexibility is given by

$$\Delta\hat{\mathbf{u}} = \mathbf{u}_0 - \sum_{i=1}^{m} \frac{\hat{\mathbf{u}}_i \hat{\mathbf{u}}_i^{\mathrm{T}} \mathbf{f}^{\star}}{\omega_i^2}\,, \tag{25}$$

where the first right-hand-side term is the static response and the second right-hand-side term is the contribution of the low frequency modes to the static response. This equation shows that the residual flexibility effect will be significant if the static response is of the same order as the dynamic response, and, the static response is not well expanded in terms of the lower modes. Since for this load case the static response is the much larger near the point location than near the piezo patch location, the residual flexibility effect is more clearly visible in Fig. 2(a). Figure 3 shows the results for the second load case. The residual flexibility effect is most clearly observed in Fig. 3(b). If this effect is not included, the error in the prediction of the anti-resonance frequencies is reasonable. In Fig. 3(b) the mismatch between the reduced models is much smaller. As for the first load case, this is because the corresponding response point is not close to the piezo patch. The results clearly show that the residual flexibility can improve the accuracy of the modal expansion, particularly for transfer functions with coinciding excitation and response points.

3. SOUND RADIATION MODEL

In order to investigate the performance of different control strategies a model that describes the interaction of the structural vibration and the radiated sound field must be available. The radiated sound power is often used in ASAC as performance metric for the controller. The time-averaged radiated acoustic power through an area S can be expressed as

$$\bar{W} = \frac{1}{2}\,\mathrm{Re}\left(\int_S p(\mathbf{r}_s)\, v_n^*(\mathbf{r}_s)\,\mathrm{d}S\right)\,, \tag{26}$$

where $p(\mathbf{r}_s)$ and $v_n(\mathbf{r}_s)$ denote respectively the surface pressure and the normal velocity on the structure at position vector $\mathbf{r}_s$. The normal velocity distribution is known from the analysis described in the previous section. It is hereby assumed that the vibration of the structure is not affected by the surrounding medium. There are several methods available to obtain the acoustic pressure, such as the boundary element method and finite element method. These are especially suited to analyse sound radiation of complex structures. In the current work the analysis is restricted to a plate in an infinite baffle. In that case the Rayleigh integral can be used to model the acoustic field.

3.1. Rayleigh Integral Method

The Rayleigh integral[5] is given by

$$p(\mathbf{r}) = \frac{\mathrm{j}\omega\rho_0}{2\pi}\int_S v_n(\mathbf{r}_s)\frac{\mathrm{e}^{-\mathrm{j}k|\mathbf{r}-\mathbf{r}_s|}}{|\mathbf{r}-\mathbf{r}_s|}\,\mathrm{d}S\,, \tag{27}$$

where ρ_0 is the mean density of the acoustic medium, $k = \omega/c_0$ is the acoustic wavenumber with c_0 the undisturbed speed of sound. Because there is normally no closed form solution available, the Rayleigh integral and thus the expression for the radiated sound power are discretised. The surface is divided into l elementary radiators (pistons) of equal size. It is assumed that the velocity and pressure fields across each radiator are constant. Then Eq. (26) reduces to the summation

$$\bar{W} = \frac{S_e}{2}\,\mathrm{Re}\left(\mathbf{v}_n^{\mathrm{H}}\,\mathbf{p}\right)\,, \tag{28}$$

where $\mathbf{p}$ and $\mathbf{v}_n$ are the vectors with the surface pressure and normal velocity of the elementary radiators, S_e is the surface of an elementary radiator, and subscript $^{\mathrm{H}}$ denotes the Hermittian. Discretisation of the Rayleigh integral leads to a linear relation of the form

$$\mathbf{p} = \mathbf{Z}\,\mathbf{v}_n\,, \qquad \text{with} \qquad Z_{ij} = \frac{\mathrm{j}\omega\rho_0 S_e}{2\pi}\,\frac{\mathrm{e}^{-\mathrm{j}k|\mathbf{r}_i-\mathbf{r}_j|}}{|\mathbf{r}_i-\mathbf{r}_j|}\,, \qquad i,j = 1\ldots l\,. \tag{29}$$

The pressure is here evaluated on the surface, meaning that the diagonal elements of impedance matrix $\mathbf{Z}$ are singular ($i = j$). The expression for the time-averaged radiated sound power now becomes

$$\bar{W} = \frac{S_e}{2}\,\mathrm{Re}\left(\mathbf{v}_n^{\mathrm{H}}\,\mathbf{Z}\,\mathbf{v}_n\right) = \mathbf{v}_n^{\mathrm{H}}\,\mathbf{R}\,\mathbf{v}_n\,, \tag{30}$$

where $\mathbf{R}$ is the radiation resistance matrix. This matrix is given by

$$\mathbf{R} = \frac{\omega^2 \rho_0 S_e^2}{4\pi c_0} \begin{bmatrix} 1 & \frac{\sin(kr_{12})}{kr_{12}} & \cdots & \frac{\sin(kr_{1l})}{kr_{1l}} \\ \frac{\sin(kr_{21})}{kr_{21}} & 1 & \cdots & \vdots \\ \vdots & \vdots & \ddots & \vdots \\ \frac{\sin(kr_{l1})}{kr_{l1}} & \cdots & \cdots & 1 \end{bmatrix} . \tag{31}$$

where $r_{ij} = |\mathbf{r}_i - \mathbf{r}_j|$. Because only the real part of the impedance matrix is used for evaluation of the radiation resistance matrix, no singularity is present.

3.2. Radiation Modes

Below coincidence, i.e. $kL < 1$ with L the characteristic length scale of the plate, the structural modes do not contribute independently to the radiated sound power. Above coincidence, the structural modes radiate more or less independently. ASAC normally focuses on the low frequency range. Thus a controller designed to reduce vibrations will not necessarily reduce the sound radiated by a structure. A set of vibration patterns can be defined which do contribute independently to the radiated sound power, the so called radiation mode shapes.[6–8] The radiation modes follow from a singular value decomposition of the radiation resistance matrix $\mathbf{R}$:

$$\mathbf{R} = \mathbf{\Sigma}^{\mathrm{T}} \mathbf{\Lambda} \mathbf{\Sigma} , \tag{32}$$

where $\mathbf{\Sigma}$ is the real matrix with radiation modes, stored row-wise, and $\mathbf{\Lambda}$ is the real diagonal matrix with radiation efficiencies. Both matrices depend on frequency. An interesting aspect is that the radiation efficiencies fall off very rapidly with increasing mode order. This makes it possible to predict the radiated sound power with only a small number of radiation modes:

$$\bar{W} \approx \mathbf{v}_n^{\mathrm{H}} \tilde{\mathbf{\Sigma}}^{\mathrm{T}} \tilde{\mathbf{\Lambda}} \tilde{\mathbf{\Sigma}} \mathbf{v}_n , \tag{33}$$

where $\tilde{\mathbf{\Sigma}}$ and $\tilde{\mathbf{\Lambda}}$ now include only a small number of modes and efficiencies. The fact that only a small number of modes is required is also interesting from a control point of view: a reduction of the participation of only a small number of radiation modes will give an optimal control performance.

3.3. Structural-Acoustic Model

In order to evaluate the radiated sound power, the normal velocity distribution on the plate is required. The normal velocity can be obtained from the state space model, but then all nodal normal velocities must be included in the output vector, which leads to a large model. Alternatively, the normal velocity can be obtained while neglecting the residual flexibility, or $\mathbf{v}_n = \tilde{\mathbf{\Psi}}_{u,n} \dot{\tilde{\mathbf{q}}}$. Matrix $\tilde{\mathbf{\Psi}}_{u,n}$ is that part of the modal matrix $\tilde{\mathbf{\Psi}}_u$ corresponding with the normal displacements. Then the radiated sound power is approximated by

$$\bar{W} \approx \dot{\tilde{\mathbf{q}}}^{\mathrm{H}} \mathbf{Q}^{\mathrm{T}} \tilde{\mathbf{\Lambda}} \mathbf{Q} \dot{\tilde{\mathbf{q}}} , \qquad \text{where} \qquad \mathbf{Q} = \tilde{\mathbf{\Sigma}} \tilde{\mathbf{\Psi}}_{u,n} . \tag{34}$$

Matrix $\mathbf{Q}$ can be calculated in advance. Every column in $\mathbf{Q}$ represents a structural mode shape expanded in terms of the radiation modes. Although not done here, it is also possible to combine the structural state space model with a state space representation of the radiation model.[9,10] Figure 4 compares three ways of computation of the radiated sound power due to a unit voltage applied to the piezo actuator (no point force). In the first approach the velocity distribution is evaluated including residual flexibility and the radiated sound power is calculated with Eq. (28) (solid line). The second method uses the same velocity vector, but the sound power is now determined with Eq. (33) using only 5 radiation modes (dash-dot line). The third result is obtained with Eq. (34), thus neglecting the residual flexibility, again using 5 radiation modes (dashed line). All results were obtained with a structural model with 12 modes. The main conclusion that can be drawn is that it is allowed to approximate the radiated sound power by Eq. (34). It was shown in Sect. 2.4 that the effect introduced by the residual flexibility can be significant when point responses are considered, and furthermore, especially near the anti-resonance frequencies. In other words, it is a local effect. Since the vibration of the whole plate area contributes to the acoustic field, the effect of residual flexibility is negligible for the radiated sound power.

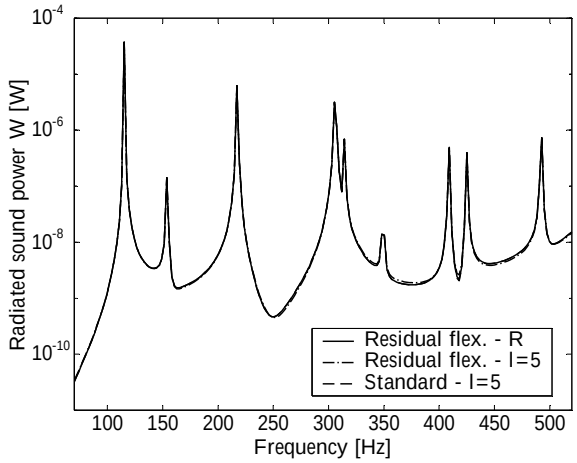

Figure 4. Comparison of three ways to calculate the sound power radiated by the plate when a unit voltage is applied to the piezo patch.

4. STRUCTURAL-ACOUSTIC CONTROL

With the model presented in the foregoing sections, the control performance of several error criteria is investigated. Optimal control theory is applied to derive the control law which minimizes a certain error criterion. This is certainly a simplified controller model, but there exist efficient and robust algorithms for realising it in practice.[11] The results presented here are again obtained for the test case defined in Sect. 2.4.

4.1. Optimal Control Theory

Optimal control theory determines the optimal response with respect to a quadratic error criterion when controlling a linear system (see for instance Nelson and Elliott[11]). It gives the optimal control performance, irrespective of the control algorithm, in case of a quadratic cost function. The frequency domain response of a linear system subjected to a number of a disturbance and control inputs can be written as

$$\mathbf{y} = \mathbf{H}_d\,\mathbf{f}_d + \mathbf{H}_c\,\mathbf{f}_c\,, \tag{35}$$

where $\mathbf{y}$ is the vector with outputs which are minimized, e.g. plate displacements, sensor voltages or pressures. Vectors $\mathbf{f}_d$ and $\mathbf{f}_c$ are the disturbance and control input vectors, respectively, and, $\mathbf{H}_d$ and $\mathbf{H}_c$ are transfer matrices which relate the disturbance and control inputs to the response. Note that $\mathbf{f}_d$ and $\mathbf{f}_c$ can contain both structural and electrical inputs. The error criterion is defined as

$$J = \mathbf{y}^{\mathrm{H}}\,\mathbf{W}\,\mathbf{y} + \beta\,\mathbf{f}_c^{\mathrm{H}}\mathbf{f}_c\,, \tag{36}$$

where $\mathbf{V}$ is the performance weighting matrix and β is a control effort penalty. The control input vector which minimizes objective equation (36) is given by

$$\mathbf{f}_c^{\mathrm{opt}} = -\left(\mathbf{H}_c^{\mathrm{H}}\mathbf{W}\,\mathbf{H}_c + \beta\,\mathbf{I}\right)\,\mathbf{H}_c^{\mathrm{H}}\mathbf{W}\,\mathbf{H}_d\;\mathbf{f}_d\,. \tag{37}$$

4.2. Control Performance

It was already mentioned that radiated sound power is an interesting error criterion for ASAC. However, it is not easy to measure this quantity in practice. Therefore, the performance of two more realistic error criteria is investigated. The first criterion uses sensors at discrete locations on the plate which measure the normal displacement $\mathbf{u}_s$. Obviously also velocity or acceleration sensors can be used. The second criterion uses a number of pressure sensors in the near-field of the plate $\mathbf{p}_s$. For both cases 6 sensors are used, see Fig. 5. The pressure sensor grid has an offset of 0.1 m with respect to the plate surface. The radiated sound power

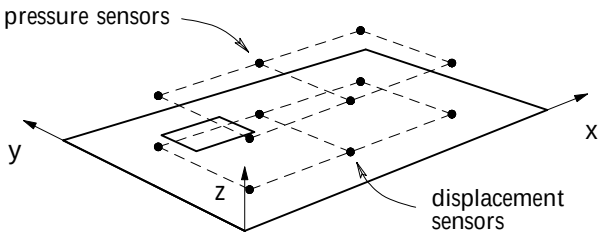

Figure 5: Schematic layout of displacement sensors and pressure sensors.

$\bar{W}$ is also used as error criterion, in order to judge the performance of the more realistic sensor layouts. The error criteria are summarized in Table 1. The table furthermore gives the output and weighting matrix used for calculation of Eq. (36) for each criterion. The pressure $\mathbf{p}_s$ is determined using the assumption that the residual flexibility effect is negligible. Because there is an offset between the plate surface and the measurement grid, the impedance matrix $\mathbf{Z}_s$ relating $\mathbf{p}_s$ to the normal plate velocity is not singular.

Table 1: Error criteria, corresponding output and weighting functions.

Objective J	Output $\mathbf{y}$	Weight $\mathbf{W}$
$\mathbf{u}_s^{\mathrm{H}}\mathbf{u}_s$	$\mathbf{u}_s$	$\mathbf{I}$
$\mathbf{p}_s^{\mathrm{H}}\mathbf{p}_s$	$\dot{\tilde{\mathbf{q}}}$	$\tilde{\mathbf{\Psi}}_{u,n}^{\mathrm{H}}\mathbf{Z}_s^{\mathrm{H}}\mathbf{Z}_s\,\tilde{\mathbf{\Psi}}_{u,n}$
$\bar{W}$	$\dot{\tilde{\mathbf{q}}}$	$\mathbf{Q}^{\mathrm{T}}\tilde{\mathbf{\Lambda}}\,\mathbf{Q}$

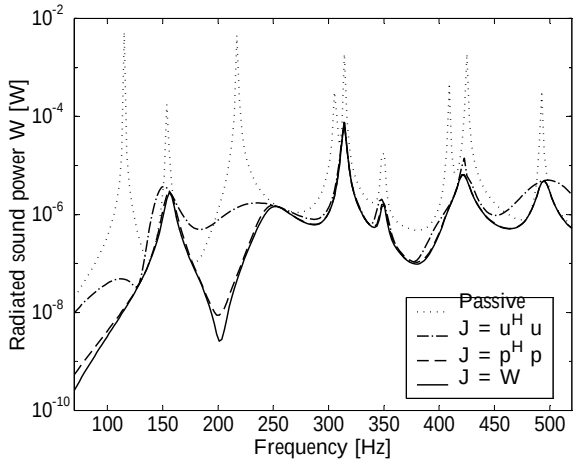

Figure 6: Comparison of radiated sound power reduction for different error criteria.

Results are presented for the same test case as discussed in Sect. 2.4. The point force is the primary or disturbance input (amplitude=0.1 N). The secondary or control input is the voltage applied to the piezo patch. For all objectives the control penalty β is set to zero. Figure 6 compares the reduction in radiated sound sound power which is realized for the different criteria. The results show that compared to the passive response a significant reduction is achieved for all criteria. The line for minimization of $\bar{W}$ (solid line) shows that the reduction at the resonance frequencies varies. This is because the controllability of a mode depends on the

piezo patch location, and is thus different for all modes. A remarkable aspect is that the minimization of the pressure at only 6 locations (dashed line) results in a reduction of the radiated power which is nearly equal to the reduction if $\bar{W}$ is minimized. The reduction which is achieved when minimizing the normal displacement shows a significant reduction at the resonance frequencies. But an increase of radiated power is observed in some off-resonant regions. In these frequency ranges the plate vibration is significantly reduced. The radiated sound power does however increase because the structural modes do not radiate independently.

5. CONCLUSIONS

A modelling approach for active structural acoustic control with piezoelectric actuators and/or sensors was presented. The finite element method is applied to make the method suitable for complex structures which cannot be modelled analytically. A model reduction technique was presented and validated for a setup consisting of a plate with one piezoelectric patch actuator. Simulation results showed that the concept of residual flexibility can improve the accuracy of the reduced model significantly. The structural model is coupled with an acoustic model based on the Rayleigh integral. The radiation modes concept is applied and the results showed that the radiated sound power is well described when only a small number of radiation modes is accounted for. The combined structural-acoustic model is a compact model requiring small simulation times. This makes the model useful for control system design. The model was applied to evaluate the control performance of several error criteria. Both structural and acoustic error criteria showed a significant improvement of the radiated sound power. The use of only a small number of pressure sensors showed a reduction in radiated sound power which nearly equals the optimal performance.

REFERENCES

1. C. Fuller, "Active control of sound transmission/radiation from an elastic plate by vibration inputs: I. Analysis," *Journal of Sound and Vibration* **136**(1), pp. 1–15, 1990.
2. E. Dimitriadis, C. Fuller, and C. Rogers, "Piezoelectric actuators for distributed vibration excitation of thin plates," *Journal of Vibration and Acoustics* **113**(1), pp. 100–107, 1991.
3. A. Benjeddou, "Advances in piezoelectric finite element modelling of adaptive structural elements: a survey," *Computers and Structures* **76**, pp. 347–363, 2000.
4. A. Preumont, *Vibration control of Active Structures*, Kluwer Academic Publishers, 1999. ISBN 0-7923-4392-1.
5. A. Pierce, *Acoustics, and Introduction to its Physical Principles and Applications*, Acoustical Society of America, 1994 edition ed., 1981.
6. G. Borgiotti, "The power radiated by a vibrating body in an acoustic fluid and its determination from boundary measurements," *Journal of the Acoustical Society of America* **88**(4), pp. 1884–1893, 1990.
7. K. Cunefare and M. Currey, "On the exterior acoustic radiation modes of structures," *Journal of the Acoustical Society of America* **96**(4), pp. 2302–2312, 1994.
8. M. Currey and K. Cunefare, "The radiation modes of baffled finite plates," *Journal of the Acoustical Society of America* **98**(3), pp. 1570–1580, 1995.
9. W. Baumann, W. Saunders, and H. Robertshaw, "Active suppression of acoustic radiation from impulsively excited structures," *Journal of the Acoustical Society of America* **90**(6), pp. 3202–3208, 1991.
10. B. Bingham, M. Atalla, and N. Hagood, "Comparison of structural-acoustic control designs on an active composite panel," *Journal of Sound and Vibration* **244**(5), pp. 761–778, 2001.
11. P. Nelson and S. Elliott, *Active Control of Sound*, Academic Press, 1992. ISBN 0-12-515425-9.

APPENDIX A. TEST CASE PROPERTIES

The results presented in this paper were obtained with the dimensions and material parameters given in Tables 2 and 3.

Table 2: Plate properties (see also Fig. 1).

Parameters	Value
Dimensions ($l_{p,x} \times l_{p,y} \times t_p$)	$490 \times 245 \times 1.2$ mm^3
Density	2710 kg m^{-3}
Young's modulus	$70.0 \cdot 10^9$ N m^{-2}
Poisson's ratio	0.3

Table 3: Piezo patch properties (see also Fig. 1).

Parameters	Value
Dimensions ($l_{pe,x} \times l_{pe,y} \times t_{pe}$)	$50 \times 30 \times 1.0$ mm^3
Location (x_{pe}, y_{pe})	260, 90 mm
Density	7760 kg m^{-3}
Elasticity coeff. (S^E_{11}, S^E_{33}, S^E_{12}, S^E_{13}, S^E_{44}, S^E_{66})	1.68, 1.90, -0.57, -0.71, 5.10, 4.50 ($\cdot 10^{-11}$) m^2 N^{-1}
Piezoelectric coeff. (d_{31}, d_{33}, d_{15})	-2.14, 4.23, 6.10 ($\cdot 10^{-10}$) m V^{-1}
Dielectric coeff. (ϵ^T_{11}, ϵ^T_{33})	9.82, 7.54 ($\cdot 10^{-9}$) F m^{-1}